Engineering Structures 201 (2019) 109788

Contents lists available at ScienceDirect

Engineering Structures

journal homepage: www.elsevier.com/locate/engstruct

Probabilistic reliability framework for assessment of concrete fatigue of existing RC bridge deck slabs using data from monitoring

Amol Mankar[a,*], Imane Bayane[b], John Dalsgaard Sørensen[a], Eugen Brühwiler[b]

[a] Aalborg University, Thomas Manns Vej, 23, 9220 Aalborg, Denmark
[b] EPFL ENAC IIC MCS, Ecole Polytechnique Fédérale de Lausanne, Switzerland

ABSTRACT

Assessment of existing bridge structures for inherent safety level or for lifetime extension purposes is often more challenging than designing new ones. With increasing magnitude and frequency of axle loads, reinforced concrete bridge decks are susceptible to fatigue failure for which they have not been initially designed. Fatigue verification and prediction of remaining service duration may turn out to be critical for civil infrastructure satisfying the required reliability. These structures are exposed to stochastic loading (e.g. vehicle loads, temperature loads); on the resistance side, reinforced concrete also behaves in a stochastic way. This paper presents a probabilistic reliability framework for assessment of future service duration, which includes probabilistic modelling of actions based on large monitoring data and probabilistic modelling of fatigue resistance based on test data. A case study for the steel - reinforced concrete slab of the Crêt de l'Anneau Viaduct is presented along with calibration of resistance partial safety factors for lifetime extension.

1. Introduction

Most of the reinforced-concrete bridges in Switzerland are more than ~60 years old. Deck slab is the high fatigue loaded part of such bridges due to the moving wheel loads [1–4]. However, such slabs may not be designed for fatigue [5]. Fatigue verification of reinforced concrete consists of (1) the verification of steel reinforcement in tension zone for tension fatigue, (2) the verification of concrete in compression zone for compression fatigue and (3) the fatigue verification of the bond between steel reinforcement and concrete [6].

Probabilistic fatigue reliability framework was used by many researchers [7–15], to estimate the fatigue safety of road and railway bridges. However these studies were limited to steel bridges or their components. They included different aspects e.g. [9] worked on the fitting of probability density functions over monitoring data for a steel bridge and concluded that, such approach worked well and produced reliable estimates of the probability of failure [13]. used six months operational strain measurement and extended the data by using Bootstrap Method [16]. [12] worked on reliability framework and replaced a complicated 3D finite element model by a response surface using theory of design and analysis of experiments & linear regression [17].

All the above-mentioned aspects related to the probabilistic modelling of actions or action effects can be used for reinforced-concrete bridge as well; e.g. the approach of fitting density functions, and response surface was used on a reinforced concrete bridge see, [18]. Quite a few researchers worked on the safety verification of reinforced-concrete and pre-stressed concrete bridges, by studying the response of reinforced-concrete material to fatigue loads. Schläfli and Brühwiler [5] conducted experimental campaign of testing 27 slab like beams (without shear reinforcement) and concluded that fatigue failure can only be observed when the fatigue load exceeds 60% of static ultimate loads. Failure was always observed on tensile reinforcement due to fracture of reinforcement and no failure on compression fatigue of concrete was observed. S-N relations of reinforcement bars were valid for estimating the life of the structures. A similar conclusion was obtained by testing corrugated steel plates and orthotropic reinforced-concrete decks under four point bending test where the failure was always observed in the welded parts of the corrugated steel plates and the corresponding S-N relations were valid for the estimating life [19]. Using the above conclusions [20], performed fatigue safety checks of a post-tensioned box-girder-road bridge. This work was limited to the deterministic domain and did not consider the compression fatigue of concrete. The safety of reinforced-concrete bridges were estimated by other approaches e.g. estimating the remaining life of bridges by linear elastic fracture mechanics of reinforcing bars [21]. [22] focused on the fretting fatigue of pre-stressing reinforcement, which occurs at the contact between pre-stressing tendons and inner surface of duct. Fatigue safety was studied using S-N curves similar to the ones of steel reinforcement.

On the other side [1–4], illustrated that, fatigue cracks in the compression side of concrete were possible. Firstly, flexural cracks get formed in the tension side of reinforced concrete and later these tensile

* Corresponding author.
E-mail address: ama@civil.aau.dk (A. Mankar).

https://doi.org/10.1016/j.engstruct.2019.109788
Received 1 January 2019; Received in revised form 7 October 2019; Accepted 10 October 2019
Available online 19 October 2019

flexural cracks get progress into the compression side due to the twisting action when a moving wheel load passes these tensile flexural cracks. This reduces shear rigidity and it further degrades deck slabs if rain water ingresses these cracks. CEB Bulletin 188 [23], illustrated seventeen case histories concerning the failure of reinforced-concrete bridge structures. For most of the cases, fatigue was the main factor contributing to the failure combined with other factors. Case histories of bridges in Holland and Japan cover failure of concrete in compression zone where reinforcement was in an intact condition. [24] conducted compression fatigue tests on cubic specimens and three point bending fatigue tests on full-scale pre-cast reinforced-concrete slabs for railway tracks.. In this study, a relation between fatigue life and secondary strain rate was developed based on test campaign. [25] covered numerical validation of tests conducted by [24]. However this study was limited to the deterministic domain. [26] considered using an artificial neural network to estimate the fatigue life of reinforced-concrete decks based on crack patterns. This study had an issue that, the training of an artificial neural network needs to cover all kind of crack patterns covering all possible failure mechanisms.

With potential fatigue damaging over time and the increase in axle loads in both aspects magnitude and frequency, the reinforced-concrete bridges often need strengthening to continue using the infrastructure with the required reliability level. Before any intervention, an assessment is necessary [5]. However, the assessment of existing bridge structures for inherent safety level or for lifetime extension purposes is often more challenging than designing new bridges. This may include updating all the uncertainties on both the action and resistance sides based on information obtained from inspections, structural interventions and monitoring campaigns conducted during the service duration of the structure. Uncertainties on the action side may include variation in vehicle weights and positions on carriageway-width of deck slabs, velocity of vehicles, number of vehicles crossing the bridge from each traffic direction, uncertainties related to temperate and related temperature induced strains. Uncertainties on the resistance side are in the form of large scatter in fatigue test data even for same conditions of test campaigns. Uncertainties in resistance also include structural response to these actions in the form of variation in action effects. Uncertainty in compressive strength of concrete relates to the gain in concrete strength over time due to continued cement hydration. To cover these wide ranges of uncertainties, the probabilistic reliability method proves to be efficient for assessing the fatigue safety of structures.

This paper presents a probabilistic reliability framework for assessment of future service duration, which includes a probabilistic modelling of actions based on monitoring data collected for a period of one year; probabilistic modelling of the fatigue resistance based on large fatigue test data compiled from literature. The probabilistic modelling of actions includes the identification and quantification of uncertainties associated with the weight of vehicles, position of vehicles and temperature inducing strain variations. This modelling is limited to the verification of the fatigue limit state only and is based on a monitoring campaign conducted for the Crêt de l'Anneau Viaduct for a period of one year and the weigh in motion (WIM) data obtained from Swiss authorities, see [18] for details about monitoring and WIM data. The probabilistic load modelling is described in Section 3. The probabilistic modelling of resistance includes a stochastic fatigue resistance model based on a wide fatigue test database available in literature; see Section 2 for details about probabilistic fatigue resistance modelling. Thus, the novelty of the paper lies with presenting a generic technique to model relation of design parameter for existing structures to calibrate partial safety factors, based on newly developed stochastic-fatigue-resistance-material-model. In addition, a case study for the Crêt de l'Anneau Viaduct is presented along with calibration of resistance partial safety factors. Calibration of resistance material partial safety factors turns to be useful for existing structures, where structural engineers can meet reliability requirements, simply by using the calibrated partial safety factors with a code-based design without performing complex reliability analyses.

2. S-N relations for concrete fatigue

2.1. Introduction

S-N relations for concrete fatigue are generally developed using data from testing campaigns. Waagaard, [27] in 1981 tested concrete for axial and flexural fatigue under different confining conditions in the presence of water (for offshore concrete foundations), see Det Norske Veritas (currently DNVGL) [27]. Cornelissen in 1986 tested concrete under tension fatigue at TU Delft, Netherlands [28]. Petkovic in 1990 tested high strength concrete during that time, which is less than 100 MPa compressive strength, for axial compression fatigue [29]. Lohaus and others tested ultra-high strength concrete with compressive strength of 180 MPa [30]. As outcome of all this research works, international codes e.g. DNV-OS-C502 [31], NEN 6723 [32], EN 1990 [33], *fib* MC1990 [34] and *fib* MC2010 [35], have proposed models for predicting fatigue service duration of concrete structures. These codes use the Palmgren-Miner (PM) rule [36,37] of linear damage accumulation where the fatigue strength is represented by a combination of Goodman Diagrams [38] and Wöhler Curves also known as S-N curves. Fatigue behaviour of concrete is governed not only by the stress range but also by the mean level of stresses. Use of the Goodman diagram to describe the fatigue behaviour accounts for the importance of the mean level of stresses.

All research papers, reports, international codes and standards agree that scatter in concrete fatigue test results has to be accounted for and proposed characteristic design curves/surfaces together with the partial safety factor concept. In order to obtain both reliable and cost-competitive design of reinforced and pre-stressed concrete structures, it is important that the uncertainty of the individual parameters is estimated and taken into account in the design process. This can to some degree be done by applying the partial safety factor approach but a much more elaborate approach can be obtained by adopting a probabilistic design approach where the structure is designed to meet a target reliability level. For this purpose uncertainty related to each parameter influencing the fatigue strength should be quantified and modelled by stochastic variables in order to estimate fatigue reliability. Thus, application of structural reliability theory could be an efficient way, to adequately-account for all these uncertainties while predicting fatigue service durations and future service durations of concrete structures [39].

2.2. Compilation- and statistical-analysis- of fatigue test data

The stochastic material model for fatigue of concrete presented in this paper is developed from a large database of concrete fatigue tests, collected from the literature, namely [40,30,29,41,42]. All compiled data and thus the developed model focuses on axial compression-compression fatigue of concrete. The database used for development of the material model consists of 600+ laboratory tests, from 10 to 11 experimenters. These tests cover a wide range of variables. For example, normal-strength concrete with compressive strength from 26 MPa to ultra-high-strength concrete with compressive strength of 226 MPa. The stress range varies from 5% to 95% of static compressive strength, tested under different range of frequencies 1–65 Hz and cover very high cycles of fatigue up to 15 million cycles. Normalized data is plotted (asterisks) see Fig. 1. A statistical analysis of the above database is performed using the fatigue strength model presented by Lohaus et al. [30], also adopted by [35]. This statistical analysis is performed using the Maximum Likelihood Method (MLM) for fitting the data to the model. Compared to other methods like least square fit, MLM has the advantage that, runout cases in fatigue tests can be included. Furthermore, it is easier to obtain Fisher information matrix and thus the parameter uncertainty associated with estimated parameters along with

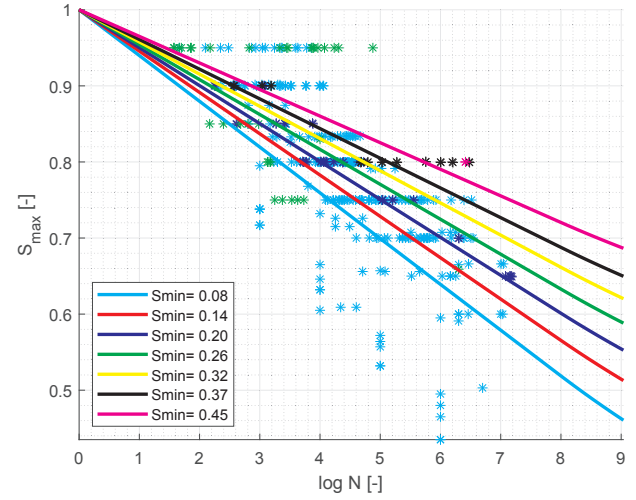

(a) fib MC2010 material model and fatigue test data

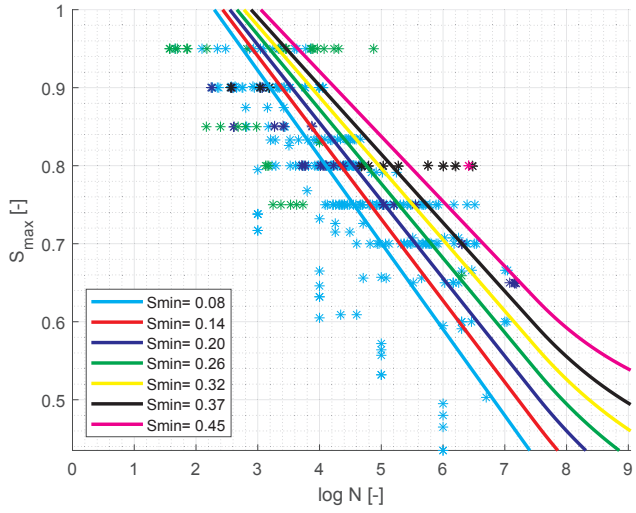

(b) Probabilistic material model (mean curves) and fatigue test data

Fig. 1. (a&b) Probabilistic material model fit comparison with fib MC2010 fit for all fatigue test campaigns.

their correlations. This information can be directly used in reliability analysis [43,44]. A local sensitivity and identifiability analyses were performed to obtain a unique set of parameters from available data, see [45], for other models, reference is also made to [46,47]. This dataset is used for obtaining a probabilistic fatigue-strength model as explained in Section 2.3, which forms as stochastic input of resistance side for reliability analysis.

2.3. Modification of existing S-N relations for better fit to the data

The *fib* MC2010 [35], is used as basis for modification to new SN-curves. The fib MC2010 [16], is used as basis since the S-N relations are formulated covering high-strength- and ultra-high-strength- concrete fatigue tests. Also fib MC2010 uses asymptotic second slope of S-N relations without any kink. The number of cycles required for failure ($\log N_{D,ij}$)at a specific maximum ($\sigma_{c,max,i}$) and minimum ($\sigma_{c,max,j}$) level of stress is given by:

$$\log N_{D,ij} = \frac{8}{(Y-1)}\cdot(S_{cd,max,i} - 1), \quad \text{if } \log N_{D,ij} \le 8$$

$$\log N_{D,ij} = 8 + \frac{8\cdot\ln(10)}{(Y-1)}\cdot(Y - S_{cd,min,j})\cdot\log\left(\frac{S_{cd,max,i} - S_{cd,min,j}}{Y - S_{cd,min,j}}\right), \quad \text{if } \log N_{D,ij} > 8 \tag{1}$$

where

$$Y = \frac{0.45 + 1.8\cdot S_{cd,min}}{1 + 1.8 S_{cd,min} - 0.3\cdot S_{cd,min}^2}$$

$$S_{cd,max,i} = \frac{\gamma_{ED}\cdot|\sigma_{c,maxi}|\cdot\eta_c}{f_{cd,fat}}$$

$$S_{cd,min,j} = \frac{\gamma_{ED}\cdot|\sigma_{c,min,j}|\cdot\eta_c}{f_{cd,fat}}$$

γ_{ED} partial safety factor for fatigue load. For sufficiently accurate stress analysis γ_{ED} can be 1.0 otherwise a value of 1.1 is recommended in [35]. For current case, γ_{ED} is considered as 1.0 as direct strain measurements are available.

η_c averaging factor for concrete stresses in the compression zone considering stress gradient.

$f_{cdfat} = \beta_{c,sus(t,t0)}\cdot\beta_{cc(t)}\cdot f_{cd}\cdot(1 - f_{cd}/400)$, is the design reference fatigue strength.

$f_{cd} = f_{ck}/\gamma_c$, in MPa.

$\sigma_{c,max,i}$ & $\sigma_{c,max,i}$ are max. and min. stresses used to obtain $S_{cd,max,i}$&$S_{cd,min,j}$.

γ_c partial safety factor for material, 1.5 is recommended in [35]

$\beta_{cc(t)}$ factor considered for strength gain over time due to continued hydration.

$\beta_{c,sus(t,t_0)}$ coefficient which takes into account the effect of high mean stresses during loading. For fatigue loading it may be taken as 0.85.

Eq. (1) presents a design equation, while the corresponding characteristic equation can be obtained by setting the resistance partial safety factor $\gamma_c = 1.0$.

Eq. (1) is slightly modified and stochastic variables are introduced in order to capture various uncertainties. The basic change adopted to Eq. (1) is that $S_{cd,max,i} = 1$ is not bound to be at $\log N_{D,ij} = 0$. This is done by replacing 1.0 with a stochastic variable X_1. This enables the failure curves to capture the data points more accurately. However, this introduces a limitation to the failure curves and the curves cannot be used for low cycle fatigue (number of cycles in order of 1000 i.e. $\log N_{D,ij} \le 3$) coupled to ultimate strengths.

Further, the assumption about the sustained compressive strength of concrete linearity until $\log N_{D,ij} = 8$ is changed in the model and instead, a stochastic variable (X_2) is introduced to take care of this linearity limit of curves. The fatigue strength reduction factors proposed ($\beta_{c,sus}$ and $1 - f_{cd}/400$) in [30,35] are not included in the probabilistic modelling since they are not supported by any test evidence, [35] & [47].

Also an un-biased error term ϵ normally distributed $N(0, \sigma_\epsilon)$ is added to take care of model uncertainty with the proposed model. All these three parameters (X_1, X_2&σ_ϵ) are estimated by using MLM. See Table 1 for their estimated mean values, parameter uncertainties and correlation coefficients among each other. See Eq. (2) which is used in MLM for fitting the curves.

$$\log N_{S,ij} = \frac{X_2}{(Y - X_1)}\cdot(S_{c,max,i} - X_1) + \epsilon, \quad \text{if } \log N_{S,ij} \le X_2$$

$$\log N_{S,ij} = X_2 + \frac{X_2\cdot\ln(10)}{(Y - X_1)}\cdot(Y - S_{c,min,j})\cdot\log\left(\frac{S_{c,max,i} - S_{c,min,j}}{Y - S_{c,min,j}}\right) \quad \text{if } \log N_{S,ij} > X_2 + \epsilon, \tag{2}$$

2.4. Comparison of new fit

Asterisks in Fig. 1 show the fatigue test results from the data base explained in Section 2.2 above. As explained in Section 2.1 fatigue test

Table 1
Stochastic parameters in limit state equation.

Area	Parameter	Distributiontype	MLE Estimation		Remark
			Mean	Std. Dev.	
Fatigue Strength Model, see Section 2.5	Δ	Lognormal	1.0	0.30	Uncertainty associated with PM rule concrete fatigue
	X_1	Normal	8.66	0.37	Limit for linearity of $logN_S$
	X_2	Normal	1.13	0.03	Value of $S_{max,i}$ at $logN_S = 0$
	ε	Normal	0.00	σ_ε	Error assumed N(0, σ_ε), Unbiased
	σ_ε	Normal	0.88	0.07	Std. Dev of Errorε
	$\rho_{X_1,\sigma_\varepsilon}$	–	0.01		Correlation coefficient obtained by MLE
	$\rho_{X_2,\sigma_\varepsilon}$	–	−0.01		Correlation coefficient obtained by MLE
	ρ_{X_1,X_2}	–	−0.84		Correlation coefficient obtained by MLE
	X_{f_c}	Log-Normal	1.00	0.20	Assumed uncertainty associated with strength of concrete f_c ++
Fatigue Load Model	X_L	Log-Normal	1.00	0.05	Uncertainty associated with stress from monitoring and obtained from ANSYS through FEM*
	ε_{temp}	Normal	10.00	15.00	Fitted distribution to observed temperature strain +
Evolution of traffic see Section 3.2.1	B_{CFT}	Normal	0.02	0.00**	Slope parameter obtained by MLM, see Section 3.2.1 for details.
	ε_{CFT}	Normal	0.00	0.05	Error parameter obtained by MLM, see Section 3.2.1 for details.
	$\rho_{B_{CFT},\varepsilon_{CFT}}$	NA	0.14	–	Correlation coefficient between B_{CFT} and ε_{CFT}

* A very low value of uncertainty is assumed as this FEM model is calibrated to monitoring data, ** A very low value but not zero, + normal distribution is fitted to the temperature strain values obtained from monitoring of one year data, ++ mean strength of concrete at age of 60 years is unknown, construction drawings specify 40 MPa strength during construction, now fcm is assumed as 50 MPa.

data has three main variables namely, mean-stress, stress-range and number of cycles required for fatigue-failure for a particular level of stress-range and mean-stress. Based on same, the data is plotted depicting number of cycles (log$N$) as function maximum level of stress in test campaign (S_{max})and different value of minimum level of the stress in same test campaign(S_{min}) shown in different colours. Further, Fig. 1 (a) shows fib MC2010 deterministic curves, while Fig. 1 (b) shows probabilistic mean curves obtained from new model explained Section 2.3. $S_{c,max,i}$ & $S_{c,min,j}$ are normalized with respect to f_{ck}(not $f_{ck,fat}$ as the fatigue strength reduction factors proposed ($\beta_{c,sus}$ and $1 - f_{cd}/400$) in [30,35] are not included in the probabilistic modelling since they are not supported by test evidence, [35] & [47]) as the mean values of concrete static strength for the tests conducted are not known. Comparison shows modified S-N curves are better fit to the data compared to *fib* MC2010 fit, and as expected they pass through centre of the data points which achieved by MLM.

Fig. 2 and Fig. 3 show a comparison of the new modified fitted curve with international codes, e.g. [31,48,34,35] for mean and characteristic strengths respectively. Fatigue tests data are also plotted (asterisks) for getting a better idea about associated strength curves. Two values of the characteristic compressive strengths (f_{ck}) are chosen for illustration such that they represent normal-strength (38 MPa) and ultra-high-strength (170 MPa) concretes.

Comparing characteristic curves is an easy task as these characteristic curves are directly shown in all codes; however, obtaining mean curves is not a trivial task, as not all assumptions made by these codes while producing the curves are known. For illustration purpose, it is assumed that the mean curves can be obtained by replacing all characteristic values of material strength in codes by the corresponding mean values. It is to be noted that, this assumption results in conservative curves, as all other constants used for obtaining the curves are kept same. The other constants mentioned before consists of constants used in formulation of S-N relations in different codes (e.g. 8, 1.8 0.45, 0.3 in *fib* MC2010 formulations, C1 in DNV formulation, 14 proposed in EN1992 or 12, 16, 8 in *fib* MC1990 formulations), are not touched upon, there are conservatism built-in these constants.

Observations from Fig. 2 (a & b): the mean SN-curves of all standards remain the same for all strengths of concrete (shown for two strengths) as they are normalized with respect to strength of concrete, see assumptions presented above. The mean SN-curves of all standards appear to be away from the fatigue test data while the modified curve passes through the data and the new fitted mean curves change for each strength of concrete as it is based on related fatigue tests. The test data is available until 15 million cycles (max), the extended part of the curves (tail of S-N curves) asymptotically reaches minimum compressive stress value, which basically shows when stress range is reduced very high number of cycles are required for failure.

Observations from Fig. 3 (a & b): Characteristic failure curves is highly influenced by the static compressive strength of concrete. All international codes are very conservative, especially with increased static strength of concrete. The proposed curves by all codes are far away from the data predicting a very low number of cycles to failure. This conservatism increases with increase in static strength of concrete as it can be seen that the SN-curve for f_{ck} of 170 MPa is much more conservative than the SN-curve obtained for f_{ck} equal to 38 MPa. DNVOSC502 is a bit less conservative compared to all other codes. Change of formulation for fatigue strength reduction based on static strength of concrete in *fib* MC2010, compared to *fib* MC1990 is reflected as large deviation in curves for high strength concrete compared to other standards [48] & [34]. EN1992, [48] and *fib* MC1990, [34] looks similar to each other.

The new characteristic SN-curve is obtained as $\log N_{SC} = \log N_S - 1.65 * \sigma_\epsilon$, where $\log N_S$ and σ_ϵ are defined by Eq. (2). While obtaining characteristic curves the uncertainty related to compressive strength is not accounted as variation in compressive strength of concrete is not available for the database considered in this study.

2.5. Specific to the Crêt de l'Anneau Viaduct

As seen in Fig. 2, the mean fitted curves vary based on the strength of the concrete. To obtain a stochastic model for fatigue of concrete for the current case study of the Crêt de l'Anneau Viaduct, fatigue test data within the range of compressive strength varying from 20 MPa to 60 MPa are used. This is considered to represent the variability in viaduct's compressive strength, which was ~40 MPa, 60 years ago. The material model formulation is detailed in Section 4.2. The stochastic parameters used to obtain the strength curves shown in Fig. 4 are listed in Table 1.

3. Stochastic action model for the Crêt de l'Anneau viaduct

Fig. 5 shows view of Crêt De l'Anneau bridge viaduct, it was commissioned in year 1957. It has eight spans with total length of 194.8 m, each span is connected to each other by articulation of steel box girder

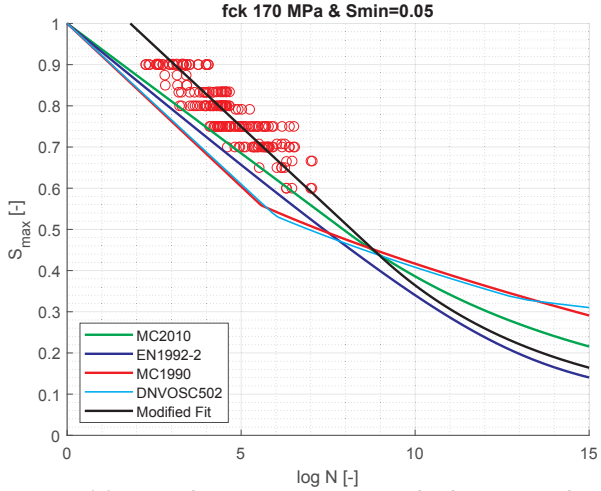

(a) Mean fatigue strength curves for f_{ck} 170 MPa for tests with S_{min}=0.05

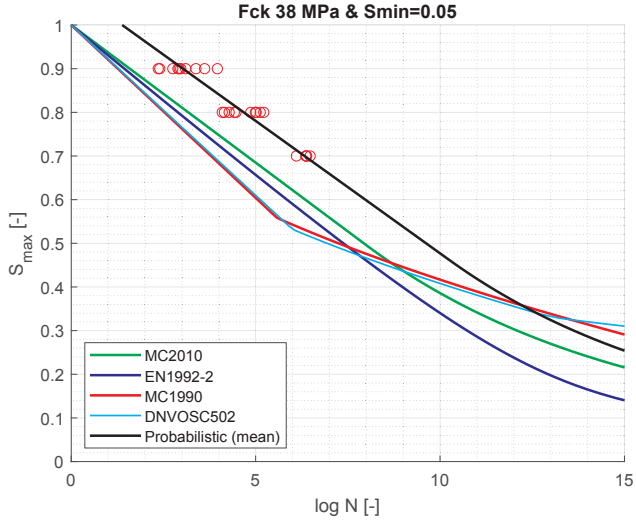

(b) Mean fatigue strength curves for f_{ck} 38 MPa for tests with S_{min}=0.05

Fig. 2. (a & b) Comparison of mean failure curves with different international codes (red dots represent corresponding fatigue test campaign) shown for two static strengths.

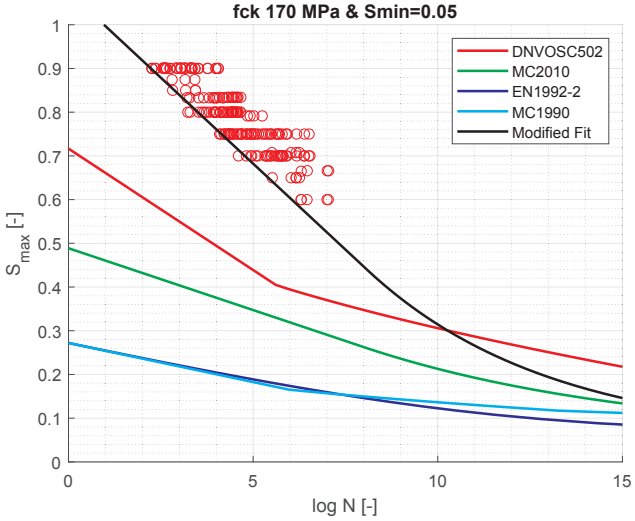

(a) Characteristic fatigue strength curves for f_{ck} 170 MPa for tests with S_{min}=0.05

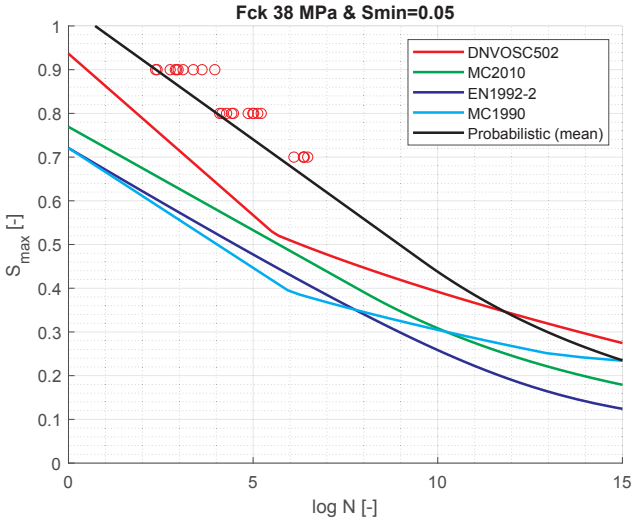

(b) Characteristic fatigue strength curves for f_{ck} 38 MPa for tests with S_{min}=0.05

Fig. 3. (a & b) Comparison of Characteristic failure curves with different international codes (red dots represent corresponding fatigue test campaign) shown for two static strengths.

beams. The carriage-way width of the deck is 12.7 m is supported transversely between two box girder beams. The deck slab has orthogonal grid reinforcement serving for double bending behaviour in transverse and longitudinal direction. The reinforcement consists of different diameters ranging from Φ10 mm, Φ14 mm and Φ18 mm forming grid in both compression and tension zone.

Strain gauges are installed on the Crêt de l'Anneau Viaduct. Continuous measurements are performed for a period of one year (from July 2016 to July 2017) with frequency of 50, 75 and 100 Hz for strains and 1 Hz for temperature and humidity. Data obtained from these continuous measurements is presented shortly in Section 3.1. Further, a stochastic load model is developed from these strain measurements, which includes stochastic variation of live load (vehicles) and stochastic variation of temperature load, is presented in Sections 3.2 and 3.3. Monitoring data obtained and development of stochastic load model are detailed in [18]. The reinforced concrete deck slab of the viaduct is governed by its transverse bending behaviour and found critical in fatigue after code-based re-calculation [49]. The action effects and stochastic model studied in further sections are limited to transverse stresses in concrete at mid-span of the viaduct in compression zone.

3.1. Action effects (Monitoring data-Strain)

Highest stresses due to live load are expected at mid-span (in the transverse direction) of the deck slab based on influence line diagram for longitudinal section of the viaduct. At this same location, strain gauges are installed on longitudinal and transverse reinforcements for the strain measurements. Strain is measured at a frequency of 50–100 Hz that captures responses due to every vehicle passing the viaduct. Along with this high frequency response of traffic, strain gauges also capture change in structural response due to ambient temperature variation [18,50].

Neutral axis for reinforced concrete section of deck slab is obtained [18] and a Markov Matrix for stresses is obtained from monitored strain in concrete for a period of one year is presented in Fig. 6.

3.2. Live load (vehicles)

Monitoring data presented in Section 0 is used to obtain weight of vehicle and its position along the carriageway width. The vehicle

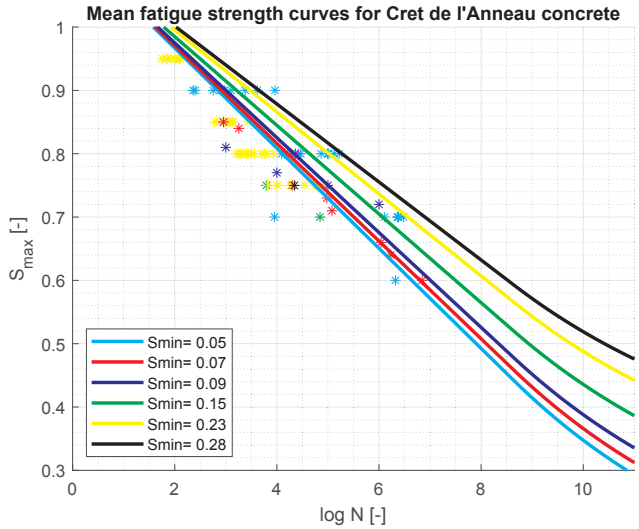

Fig. 4. Mean fatigue failure curves for concrete for the RC slab of the Crêt De l'Anneau Viaduct.

weight and the position is back calculated based on the calibration test performed for the viaduct with a truck of 40 Metric Tonne (MT) of known axle weights, [49]. The logic behind back calculation is detailed in [18].

The stochastic variation of live loads is presented in the form of weight distributions of vehicles and vehicle positions on carriageway width of the viaduct, see Fig. 7. A vehicle is described by its weight and position and both these variables are correlated to each other. However, to cover more possibilities which might not been captured in one year of measurements, these variables are modelled as un-correlated. Then, the probability of vehicle with specific weight (W) at specific position (P) can be calculated as simple product of these two probabilities, see Eq. (3).

$$P_{ij} = P\left[\left(P_{B_{C,i}} - \frac{P_{B_W}}{2}\right) \le P \le \left(P_{B_{C,i}} + \frac{P_{B_W}}{2}\right)\right] \cdot P\left[\left(W_{B_{C,j}} - \frac{W_{B_W}}{2}\right) \le W \le \left(W_{B_{C,j}} + \frac{W_{B_W}}{2}\right)\right] \quad (3)$$

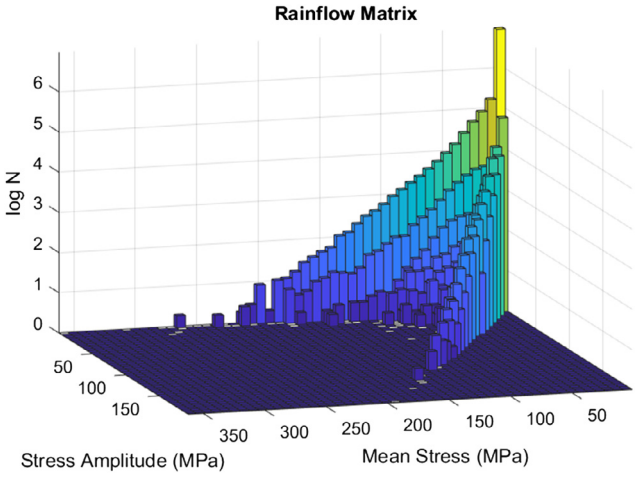

Fig. 6. Markov matrix for strain in concrete at mid-span of the viaduct.

where $P_{B_{C,i}}$ is i^{th} bin-centre for the position with bin width of P_{B_W} while $W_{B_{C,i}} j^{th}$ bin-centre for the weight with bin width of W_{B_W}.

Eighty-five bins of 100 mm size each are used for description of vehicle positions while sixty-four bins of 1.0 MT each are used for description of vehicle weight.

Finite Element (FE) model in ANSYS is used to obtain the response of the structure for each position and weight of the vehicle covering all possibilities i.e. 5440 (85 × 64). The FE model is detailed in [18].

3.2.1. Evolution of traffic with time

Traffic data are obtained from two Swiss authorities for the years from 2002 to 2016 and plotted as shown in Fig. 8, see [18] for details. Traffic growth is plotted as the ratio of number of vehicles versus years in which the traffic is observed. This ratio is normalized with respect to the number of vehicles observed in year 2016. A MLM estimate is obtained using the linear model shown in Eq. (4).

$$traffic(t) = A_{CFT} + B_{CFT} \cdot t + \epsilon_{CFT} \quad (4)$$

where t is the lifetime of the structure, A_{CFT} is an intercept parameter and B_{CFT} is a slope parameter. ϵ_{CFT} models the error in estimate and its unbiased estimate so ϵ_{CFT} $N(0, \sigma_{\epsilon_{CFT}})$. All the three parameters (A_{CFT}, B_{CFT} and $\sigma_{\epsilon_{CFT}}$) are modelled as uncertain parameters describing the trend of the traffic. However, it was observed that, A_{CFT} and B_{CFT}

Fig. 5. Crêt De l'Anneau: the investigated steel-concrete composite viaduct.

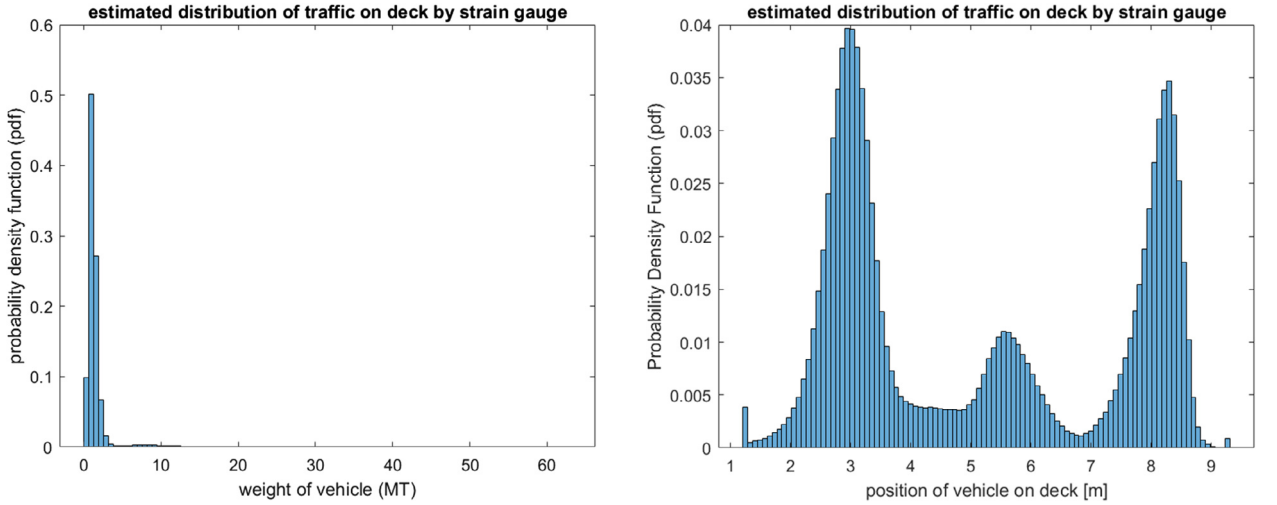

(a) Traffic weight distribution (b) Traffic position distribution along the width of viaduct

Fig. 7. Weight and Position Distribution (along carriageway width) of vehicular traffic on the Crêt de l'Anneau Viaduct.

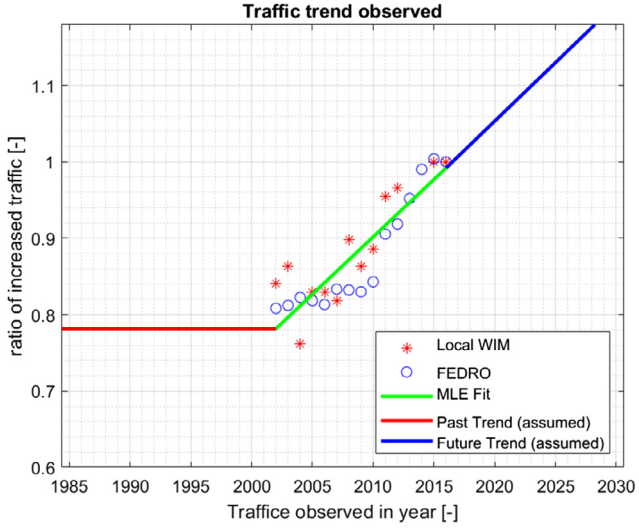

Fig. 8. Traffic trend modelled based on available data for the Crêt de l'Anneau Viaduct*.

are highly correlated with correlation coefficient close to unity so A_{CFT} is fixed and B_{CFT} & $\sigma_{\epsilon_{CFT}}$ are obtained from MLE (see Table 1).

Traffic trend is assumed to follow same growth in number of vehicles after year 2016 with the same level of uncertainty, while past traffic is assumed with the same number of vehicles as of year 2002 with the same level of uncertainty (this is a conservative assumption due to lack of data on past traffic), see Fig. 8.

3.3. Action model for temperature variation

The stochastic variation of temperature is captured by thermometers installed in concrete part of the viaduct and related temperature strains derived from monitoring data (see Fig. 9). The temperature strain can be easily separated from observed monitoring data as vehicles have very high frequency change in strain compared to temperature, see [18]. A normal distribution fits well for temperature strain and it can be easily used in a reliability analysis.

4. Assessment equation and limit state equation

Reliability analyses are performed for two load models: (1) strains obtained from monitoring (action effects, Section 0) are used directly; (2) strains obtained from the numerical model (ANSYS) is used for the stochastic load model described in Section 3.2. Rain-flow counting of stress history (see Markov matrix Section 0) based on strain obtained from monitoring is performed in order to estimate the number of cycles, stress-range and mean-stress levels. These form input for assessment Eq. (5). Strains observed in monitoring are assumed to be very accurate information with COV 5% and is modelled as lognormal distribution; see Table 1, this stochastic variable is an input for limit sate Eq. (6). The vehicle position and weight are input parameters for ANSYS model to obtain stresses/strains for that particular position and weight. As the ANSYS model is calibrated to yield the same results as those obtained by monitoring, it is assumed that ANSYS results have same uncertainty of COV = 5% and is modelled by a lognormal distribution, see Table 1. For both the cases, the assessment equation and limit state equation remain the same with just with the change of stress inputs.

4.1. Assessment equation

An assessment Eq. (5) is formulated using the Miner's rule of linear damage accumulation and Eq. (2).

$$G(T_L) = 1 - Damage = 1 - \sum \frac{n}{N} = 1 - \sum_{i=1}^{N_{Smax}} \sum_{j=1}^{N_{Smin}} \frac{C_{FT} \cdot n_{ij} \cdot T_L}{N_{Dij}} \quad (5)$$

where

T_L service duration of the structure.

N_{Smax} and N_{Smin} are the number of bins for $S_{Cd,max}$ and $S_{Cd,min}$ respectively.

n_{ij} experienced/observed number of stress cycles of $S_{Cd,max,i}$ and $S_{Cd,min,j}$ in each bin (i, j) per year.

$N_{D,ij}$ required number of stress cycles of $S_{Cd,max,i}$ and $S_{Cd,min,j}$ in each bin (i, j) per year for failure calculated deterministically based on Eq. (1).

C_{FT} Section 3.2.1.

$\sigma_{c,max,i}$ and $\sigma_{c,min,j}$ are maximum and minimum stresses.

$\sigma_{c,max,i} = DPR_{DL} \cdot \sigma_{DL} + DPR_{LL} \cdot X_L \cdot \sigma_{LL,max} + DPR_{temp} \cdot \sigma_{temp}$.

$\sigma_{c,min,j} = DPR_{DL} \cdot \sigma_{DL} + DPR_{LL} \cdot X_L \cdot \sigma_{LL,min} + DPR_{temp} \cdot \sigma_{temp}$.

σ_{DL} the stress due to dead load of the viaduct.

σ_{LL} the stress due to vehicle load on the viaduct and is obtained for two cases first for case of monitoring and second for stochastic load model input to FEM.

σ_{temp} is the stress due to temperature effect on the viaduct,

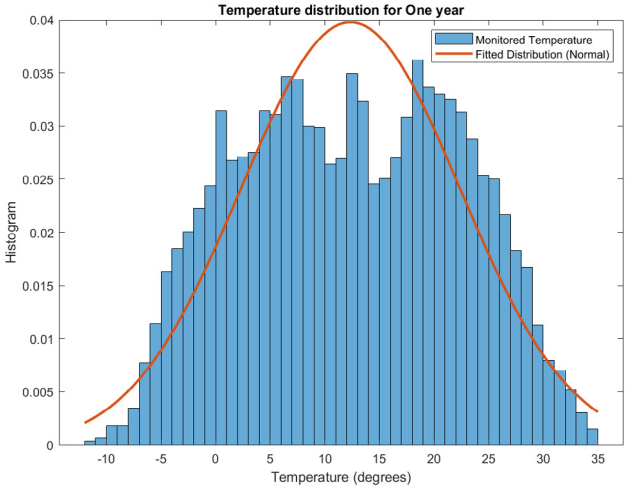

(a) Temperature data for one year observed to follow normal distribution

(b) Temperature strain data for one year observed to follow normal distribution

Fig. 9. Temperature variation and temperature strain variation in concrete part of the Crêt de l'Anneau Viaduct.

$\sigma_{temp} = \epsilon_{temp} \cdot E_c$.

ϵ_{temp} is the measured strain due to temperature.

E_c is the modulus of elasticity of concrete in MPa, $Ec = 4700\sqrt{f_{ck}}$.

f_{ck} is the characteristic static compressive strength of concrete in MPa.

DPR a coefficient that models relation between stress ratio and design parameter, see Section 4.3.

4.2. Limit state equation

A limit state Eq. (6) corresponding to the assessment Eq. (5) and Eq. (2) can be formulated by introducing stochastic variables.

$$g(t) = \Delta - \sum_{i=0}^{N_{Smax}} \sum_{j=1}^{N_{Smin}} \frac{C_{FT} \cdot n_{ij} \cdot t}{N_{S,ij}} \tag{6}$$

where

Δ model uncertainty associated with PM rule.

t time in years $0 < t < T_L$.

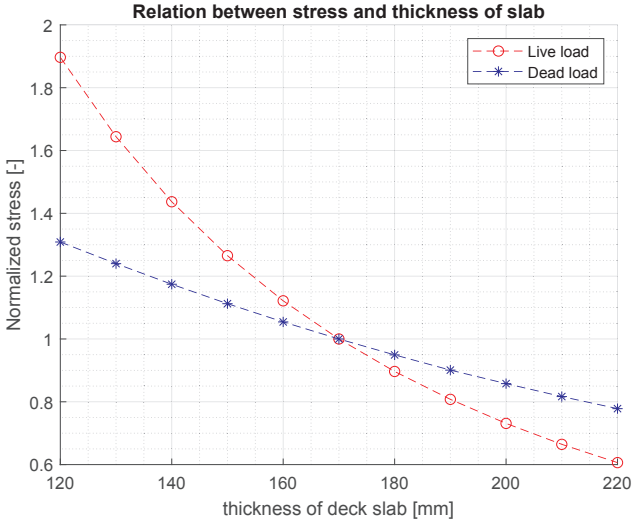

Fig. 10. Variation in stresses (due to dead load and live load) vs variation in Design parameter (Thickness of Deck Slab).

4.3. Modelling relation between design parameter and stresses

Modelling the relation between the stress values (mean and amplitude or minimum and maximum) and the design parameter is not trivial as changing the design parameter has different effects on mean level of the stresses and amplitudes of the stress history. To model the effect of change of a design parameter, maximum and minimum stresses are further decomposed to dead load, live load and temperature load. The effects of change of the design parameter on each of the stresses (σ_{DL}, σ_{LL} & σ_{temp}) are modelled individually. The principle of superposition can be assumed satisfied here and sequence of load application does not matter as all these loads are still in linear range, as this was verified during the calibration tests of the viaduct by MCS department of EPFL, Lausanne by load testing using a 40 MT truck with no permanent deformations observed [49]. The design parameter considered in the current study is the thickness of deck slab. Fig. 10 shows the relation between change in design parameter and change of stresses. Fig. 10 depicts also that, increasing the thickness of the slab reduces the live load stresses and the dead load stresses, but at a different rate. The increase in thickness increases of the bending stiffness of the deck slab, which reduces the stresses. However, for dead load the rate of decrease in stresses is lower as increase in thickness has also the opposite effect that it increases the weight of the slab. The effect on temperature stresses of changing the design parameter is assumed the same as the live load stresses. It is also possible to consider other design parameters e.g. tensile reinforcement in the deck slab, and then its relation with changes of stresses will generally be different from that of thickness of the deck slab.

5. Reliability analysis

Current viaduct was commissioned for public use in 1957 (~60 years back) and in this paper, it is assumed to be used for 60 more years, i.e. in total of 120 years of service duration. The reliability of reinforced concrete deck slab is assessed for fatigue failure of concrete in compression and the results are presented below. Current work focuses on reliability of viaduct for fatigue failure of concrete in compression only, as fatigue reliability of reinforcement in tension is already investigated [50]. The First Order Reliability Method (FORM) is used for calculation of probability of failure, [44] & [43]. An open source Matlab-based toolbox namely, the FERUM (Finite Element Reliability Using Matlab) is used for performing all FORM calculations [51].

The cumulative (accumulated) probability of failure in time interval [0,t] is obtained by Eq. (7):

$$P_F(t) = P(g(t) \le 0) \tag{7}$$

The probability of failure is estimated by FORM, see (Madsen et al., 2006). The corresponding reliability index $\beta(t)$ is obtained by Eq. (8):

$$\beta(t) = -\phi^{-1}(P_F(t)) \tag{8}$$

where, Ð¤() is standardized normal distribution function.

The annual probability of failure is obtained based on cumulative probability of failure, see Eq. (9):

$$\Delta P_F(t) = P_F(t) - P_F(t - \Delta t), \quad t > 1 \ \ year \tag{9}$$

where $\Delta t = 1$ year. The corresponding annual reliability index is denoted $\Delta\beta$.

5.1. Code requirements for reliability

The Swiss standard (SIA-269, 2016), [52], provides guidelines for assessing the safety of existing structures. It uses a probabilistic approach and presents a target reliability level in the form of reliability indices based on consequence of failure and efficiency of interventions. Efficiency of safety-related interventions, expressed as the ratio of risk reduction to safety costs, which is similar to relative cost of safety measure explained in probabilistic model code JCSS, [53]. Low efficiency of intervention is assumed considering cost to rehabilitate an existing structure as very high and consequences of structural failure are assumed to be serious which leads to a target annual reliability of 3.7.

5.2. Effect of different uncertainties on reliability index

Uncertainty considered in Miner's rule is 0.3 is based on test data for fatigue of steel, [46,47], as a reference value, however this value for concrete may be different. A sensitivity study shows that, uncertainty on Miner's rule (Δ) is not important.

5.3. Calibration of resistance partial safety factor:

fib MC2010 recommends a partial safety factor (γ_{ED}) on fatigue loads as 1.1 and for sufficiently accurate stress analysis, this may be taken as 1.0; see section 4.5.2.3 of *fib* MC2010 [35]. For current case, very accurate strain measurements are available, so γ_{ED} it considered as 1.0.

The partial safety factor for resistance (concrete compression strength) γ_c for persistent or transient loading is recommended as 1.5 in *fib* MC2010, [35]. The definition of this partial safety factor in case of fatigue design is the ratio of design-fatigue-reference strength to characteristic-fatigue-reference strength obtained as follows see Eq. (10); see also equations 5.1–110 and 7.4–4 in *fib* MC2010, [35].

$$\mathrm{Y}_M = \mathrm{Y}_C = \frac{f_{ck,fat}}{f_{cd,fat}} \tag{10}$$

Relationship between the partial safety factor for material strength γ_c and annual reliability index $\Delta\beta$ can be obtained by using the design equation, see Eq. (5) and the limit state equation, see Eq. (6). The design parameter is the only connection between these two equations, which for the current case is thickness of the deck slab. To obtain different values of γ_c each time design parameter is set to a value such that, design-Eq. (5) is exactly fulfilled.

Thus, the relation between annual reliability index and resistance partial safety factor is presented in Fig. 11. Target reliability indices indicated in (*fib*, MC2010) [35], (SIA-269, 2016), [52] and (EN 1990, 2002), [33] can be compared to have an idea about resistance partial safety factor behind these requirements. The results shown in Fig. 11 correspond to CoV_{X_L} of 0.05 for T_L of 120 years. The uncertainty

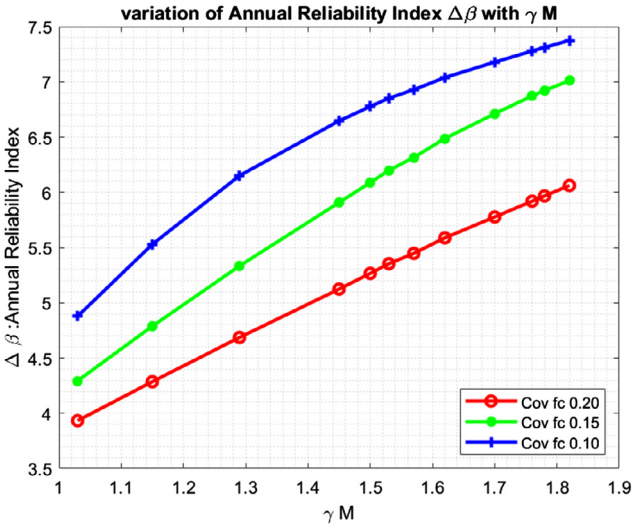

Fig. 11. Variation in annual reliability index with γ_M for TL 120.

associated with stress values obtained also plays an important role in reliability of the structure similar to uncertainty on compressive strength of concrete and therefore γ_{ED} can depend on CoV_{X_L}.

From Fig. 11 it can be seen that, a resistance partial safety factor of ~1.0 is required to achieve an annual reliability index of 3.7 when CoV_{f_c} is 0.2. It is further reduced to value less than 1.00 to achieve same criteria when, a more accurate information on concrete strength is available. It is to be noted that these conclusions are assuming a very accurate information (due to direct strain monitoring) on action effects is available ($\mathrm{CoV}_{X_L} = 0.05$). The reliability index is equally sensitive to uncertainty associated with stresses (action effects) i.e. CoV_{X_L}.

5.4. Comparison for two load models

Reliability analysis is performed for the two load models as described in Section 0, 3.2 and 4. The results are compared to see the effect of non-correlation between vehicle weight and position as described in Section 3. The difference between the two models is that model 1 uses direct strains obtained from monitoring for vehicles (for a specific weights and specific positions), while model 2 uses back calculated weight of vehicles by FEM [18] at every possible position of carriage-way width of the viaduct. Fig. 12 shows the variation of annual

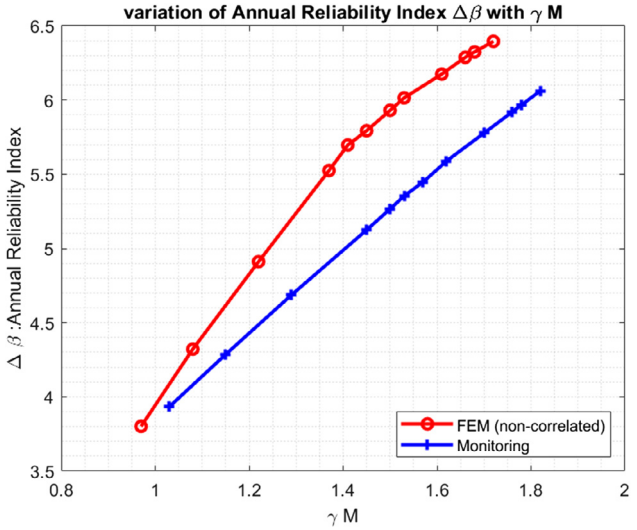

Fig. 12. Annual reliability index as function of γ_M for TL 120 and CoV_{f_c} 0.2.

reliability index ($\Delta\beta$) for both cases. There is a large difference between the reliability indices, as the characteristic stresses obtained in both cases in same way and also uncertainty with FEM is also assumed same as monitoring (since FEM is calibrated to monitoring), the reason for this variation in reliability indices may be that the current position of the vehicles (model 1, monitoring) are more critical as they pass near the centre of carriageway width while for non-correlated model (model 2, FEM) they are distributed over entire carriageway, which is yielding lower stresses and thus higher reliability. In Fig. 12 it can be seen that, for the same value of resistance partial safety factor a higher annual reliability can be obtained for FEM case. Thus distributing the weight of vehicle over entire carriageway width does not produce critical results for this case and considered fatigue critical location.

5.5. Scientific contribution, conclusion and future work

The current study proposes a methodology for the fatigue reliability assessment of existing reinforced concrete structures which includes a new stochastic SN model for fatigue of concrete, two different traffic models (action effect models), a new concept of modelling of relation between assessment parameter and stresses in concrete for existing structures. The new stochastic SN model captures fatigue test data (Section 2.2) more accurately and thus reduce model uncertainty.

Two factors play a very important role in assessment of the reliability level for fatigue of concrete structures namely the accuracy in estimating the fatigue action effects and the uncertainty related to the static compressive strength of concrete. For the considered case a very accurate information on action effects is available. However, accurate information on the static compressive strength is lacking. Also, static compressive strength of the concrete improves over the years. The accurate information about this gain in strength of concrete is unknown, unless a Non Destructive Test (NDT) is performed. It is recommended that a NDT should be performed to obtain the static compressive strength of the concrete before exercising lifetime extension decisions based on assessment of the reliability with respect to fatigue failure of the concrete.

Current study focuses on component level reliability, however an approach considering the system reliability would be helpful for inspection planning and maintaining a consistent safety of the whole structure throughout planned fatigue service duration.

Declaration of Competing Interest

The authors declare that they have no known competing financial interests or personal relationships that could have appeared to influence the work reported in this paper.

Acknowledgments

Current work is carried out under the project INFRASTAR (infrastar.eu), which has received funding from the European Union's Horizon 2020 research and innovation programme under the Marie Skłodowska-Curie grant agreement No 676139. The grant is gratefully acknowledged.

References

[1] Okada K, Okamura H, Sonoda K. Fatigue failure mechanism of reinforced concrete bridge deck slabs. Transport Res Record 1978.
[2] Perdikaris PC, Beim S. RC bridge decks under pulsating and moving load. Struct Eng 1988;114(3):591–607.
[3] Maekawa K, Gebreyouhannes E, Mishima T, An X. Three-dimensional fatigue simulation of RC slabs under traveling wheel-type loads. Adv Concr Technol 2006;4(3):445–57.
[4] Gebreyouhannes E, Chijiwa N, Fujiyama C, Maekawa K. Shear fatigue simulation of RC beams subjected to fixed pulsating and moving loads. Adv Concr Technol 2008;6(1):215–26.
[5] Schläfli M, Brühwiler E. Fatigue of existing reinforced concrete bridge deck slabs. Eng Struct 1998;20(11):pp.
[6] Mallet GP. Fatigue of Reinforced Concrete (State of the Art Review), Stationery Office Books (TSO), 1991.
[7] Chen ZW, Xu YL, Wang XM. SHMS-based fatigue reliability analysis of multiloading suspension bridges. J Struct Eng 2012;138:3.
[8] Krejsa M. Probabilistic reliability assessment of steel structures exposed to fatigue. Safety, Reliability and Risk Analysis: Beyond the Horizon; 2014.
[9] Kwon K, Frangopol DM. Bridge fatigue reliability assessment using probability density functions of equivalent stress range based on field monitoring data. Int J Fatigue 2010;32:1221–32.
[10] Ye XW, Ni YQ, Wong KY, Ko JM. Statistical analysis of stress spectra for fatigue life assessment of steel bridges with structural health monitoring data. Eng Struct 2012;45(2012):166–76.
[11] Li H, Frangopol DM, Soliman M, Xia H. Fatigue reliability assessment of railway bridges based on probabilistic dynamic analysis of a coupled train bridge system. J Bridge Eng 2016;142:3.
[12] Liu Y, Xiao X, Lu N, Deng Y. Fatigue reliability assessment of orthotropic bridge decks under stochastic truck loading. Shock Vib 2016;2016:10.
[13] Saberi MR, Rahai AR, Sanayei M, Vogel RM. Bridge fatigue service-life estimation using operational strain measurements. J Bridge 2016;21(5).
[14] Zhang W, Cai CS. Reliability-based dynamic amplification factor on stress ranges for fatigue design of existing bridges. J Bridge Eng 2013;18(6):538–52.
[15] Liu Y, Zhang H, Li D, Deng Y, Jiang N. Fatigue reliability assessment for orthotropic steel deck details using copulas: Application to nan-Xi yangtze river bridge. J Bridge Eng 2018;23:1.
[16] Efron B. Bootstrap methods: another look at the jackknife. Ann Statist 1979;7(1):1–26.
[17] Montgomery DC. Designa and analysis of experiments. westford, USA: John Wiley & Sons, Inc.; 2017. 1013.
[18] Bayane I, Mankar A, Bruhwiler E, Sørensen JD. Quantification of traffic and temperature effects on the fatigue safety of a reinforced-concrete bridge deck based on monitoring data. Eng Struct 2019;196.
[19] Ahn J-H, Sim C, Jeong Y-J, Kim S-H. Fatigue behavior and statistical evaluation of the stress category for a steel–concrete composite bridge deck. J Constr Steel Res 2008;65(2009):373–85.
[20] Treacy MA, Brühwiler E. A direct monitoring approach for the fatigue safety verification of construction joint details in an existing post-tensioned concrete box-girder bridge. Eng Struct 2015;88(2015):189–202.
[21] Rocha M, Brühwiler E. Prediction of fatigue life of reinforced concrete bridges using fracture. Bridge Mainten Saf, Manage, Resilien Sustain 2012.
[22] Casas JR, Crespo-Minguillon C. Probabilistic response of prestressed concrete bridges to fatigue. Eng Struct 1998;20(11):940–7.
[23] CEB. Fatigue of concrete structures - State of Art Report. CEB Zurich; 1988. p. 1989.
[24] Tarifa M, Zhang X, Ruiz G, Poveda E. Full-scale fatigue tests of precast reinforced concrete slabs for railway tracks. Eng Struct 2015;100(2015):610–21.
[25] Poveda E, Yu RC, Lancha JC, Ruiz G. A numerical study on the fatigue life design of concrete slabs for railway tracks. Eng Struct 2015;100(2015):455–67.
[26] Fathalla E, Tanaka Y, Maekawa K. Remaining fatigue life assessment of in-service road bridge decks based upon artificial neural networks. Eng Struct 2018;171(2018):602–16.
[27] Waagaard K. Fatigue strength of offshore concrete structures. Hovik, Norway: Det Norske Veritas; 1981.
[28] Cornelissen HAW. Fatigue failure of concrete in tension. Stevinweg 4, P.O. Box 5048, 2600 GA Delft, The Netherlands, 1986.
[29] Petkovic G, Stemland H, Rosseland S. Fatigue of high strength concrete. American Concrete Institute (International Symposium). 1992. p. 505–25.
[30] Lohaus L, Oneschkow N, Wefer M. Design Model for fatigue behaviour of normal-strength, high-strength and ultra-high-strength concrete. Struct Concr 2012.
[31] DNV OS C 502, DNV OS C 502, Offshore concrete structures. DNVGL, Høvik, Sept, 2012.
[32] NEN 6723. Regulations for concrete - Bridges - Structural requirements and calculation methods. Netherlands; 2009.
[33] EN 1990. EN 1990 Basis of structural Design," European committee for standardisation, Brussels; 2002.
[34] fib MC1990. FIB Model Code for concrete structures 1990. Berlin; 1993.
[35] fib MC2010. FIB Model Code for concrete structures 2010. Ernst & Sohn, Berlin Germany; 2013.
[36] Palmgren A. Die lebensdauer von kugellagern (The life of ball bearings). Z Ver Dtsch Ing 1924;68(14):339–41.
[37] Miner MA. Cumulative damage in fatigue. Am Soc Mech Eng – J Appl Mech 1945;12(3):159–64.
[38] Goodman J. Mechanics applied to engineering. Longman, Green & Company; 1899.
[39] Byung HO. Fatigue analysis of plain concrete in flexure. Struct Eng 1986;112(2):273–88.
[40] Lantsought E. Fatigue of Concrete under compression Database and proposal for high strength concrete. Delft: TU-Delft; 2014.
[41] Sørensen EV. Fatigue life of high performance grout in dry and wet environment for wind turbine grouted connections. Aalborg: AAU; 2011.
[42] Thiele M. Experimentelle Untersuchung und Analyse der Schädigungsevolution in Beton unter hochzyklischen Ermüdungsbeanspruchungen. Berlin: BAM; 2016.
[43] Sørensen JD. Notes in Structural Reliability Theory and Risk Analysis. Aalborg University; 2011.
[44] Madsen HO, Krenk S, Lind NC. Methods of Structural Safety. New York: Dover Publications; 2006.
[45] Aankar M, Rastayesh S, Sørensen JD. Sensitivity and Identifiability Study for Uncertainty Analysis of Material Model for Concrete Fatigue. In: IRSEC 2018,

Shiraj, 2018.
[46] Marquez-Domínguez S, Sørensen JD. Probabilistic Fatigue Model for Reinforced Concrete Onshore Wind Turbine Foundations. In: Safety, Reliability and Risk Anaysis: Beyond the Horizon ESREL 2013, Amsterdam, 2013.
[47] Slot RMM, Andersen T. Fatigue behavior and reliability of high strength concrete. Denmark: Aalborg; 2015.
[48] EN 1992-1. Design of concrete structures - Part 1-1: General rules and rules for buildings. European committee for standardisation, Brussels; 2004.
[49] MCS. Surveillance du Viaduc du Crêt de l'Anneau par un monitoring à longue durée. MSC, Lausanne; 2017.
[50] Mankar A, Rastayesh S, Sørensen JD. Fatigue Reliability analysis of Cret De l'Anneau Viaduct: a case study. Struct Infrastruct Eng 2019.
[51] FERUM. Finite Element Reliability Using Matlab; 2010.
[52] SIA-269. Existing structures – Bases for examination and interventions. Swiss Society of Engineers and Architects, P.O. Box, CH-8027 Zurich; 2016.
[53] JCSS. JCSS PROBABILISTIC MODEL CODE. JCSS; 2000.